JOURNAL OF GEOPHYSICAL RESEARCH, VOL. 107, NO. D23, 4727, doi:10.1029/2001JD002047, 2002

Simulating summertime rainfall variability in the North American monsoon region: The influence of convection and radiation parameterizations

Jianjun Xu and Eric E. Small

Department of Earth and Environmental Science, New Mexico Institute of Mining and Technology, Socorro, New Mexico, USA

Received 29 December 2001; revised 1 April 2002; accepted 12 June 2002; published 14 December 2002.

[1] Studying the dynamics of the North American Monsoon System (NAMS) is essential for understanding and assessing the predictability of its variability. Limited-area models are potentially useful tools for this endeavor, but it is important to first identify the suite of physical parameterizations that yields the most realistic simulations. We investigate how different convection and radiation schemes influence simulations of the NAMS produced with the MM5/OSU model. We focus on the simulated intraseasonal variability associated with monsoon onset (June to July) and changes between a wet (1999) and a dry (2000) year. We test six parameterizations, including two convection schema (Grell and Kain-Fritsch) and three radiation schema (CCM2, Cloud, and RRTM). We compare results from 2-month-long simulations to observations of circulation (NCEP Reanalysis) and rainfall (CPC and CMAP). Differences in simulated rainfall produced by the various combinations of schema are substantial, and much greater than the differences that arise from internal model variability in a three-member ensemble of Grell-RRTM simulations. The Grell-RRTM simulation produces the most realistic patterns and magnitudes of rainfall, including intraseasonal variations and the differences between the wet and dry year. Simulations using the Kain-Fritsch scheme produce too much rainfall, and fail to represent the atypical, observed decrease in precipitation from June-to-July in 2000. The CCM2 radiation scheme produces a simulated climate that is too cloudy, yielding little rainfall in the NAMS region regardless of the convection scheme used. The Cloud and RRTM radiation schemes allow for feedbacks between condensation and the water content of clouds, which yields substantial improvements in the model simulations. *INDEX TERMS:* 3314 Meteorology and Atmospheric Dynamics: Convective processes; 3329 Meteorology and Atmospheric Dynamics: Mesoscale meteorology; 3337 Meteorology and Atmospheric Dynamics: Numerical modeling and data assimilation; 3354 Meteorology and Atmospheric Dynamics: Precipitation (1854); 3359 Meteorology and Atmospheric Dynamics: Radiative processes; *KEYWORDS:* North American monsoon system, MM5 model, cumulus and radiation schemes, precipitation variability

Citation: Xu, J., and E. E. Small, Simulating summertime rainfall variability in the North American monsoon region: The influence of convection and radiation parameterizations, *J. Geophys. Res.*, *107*(D23), 4727, doi:10.1029/2001JD002047, 2002.

1. Introduction

[2] A large fraction of the annual precipitation in the southwestern U.S. and northwestern Mexico occurs between July through September, associated with a seasonal shift in synoptic-scale circulation patterns [*Bryson and Hare*, 1974; *Tang and Reiter*, 1984; *Rowson and Colucci*, 1992; *Douglas et al.*, 1993; *Mock*, 1996; *Adams and Comrie*, 1997]. This summertime precipitation maximum is attributed to the North American monsoon system (NAMS) (Figure 1). The onset of monsoonal precipitation is abrupt, although the date of onset varies spatially and from year to year [*Higgins et al.*, 1997]. Onset typically occurs between mid-to-late June and early July. Relatively heavy rainfall persists throughout July and August, and into September in some years.

[3] Intraseasonal and year-to-year fluctuations of summertime rainfall within the NAMS region are dramatic. Accurate predictions of these variations, with lead times of at least a month, would help mitigate their negative impacts. This requires identification of the mechanisms that produce this variability [*Gutzler and Preston*, 1997]. *Higgins et al.* [1999] found that precipitation variability in the NAMS region is linked to conditions in the eastern tropical Pacific: Positive (negative) SST anomalies favor wet (dry) winter/spring conditions and dry (wet) summer conditions. Interactions between the land surface and the atmosphere

0148-0227/02/2001JD002047$09.00

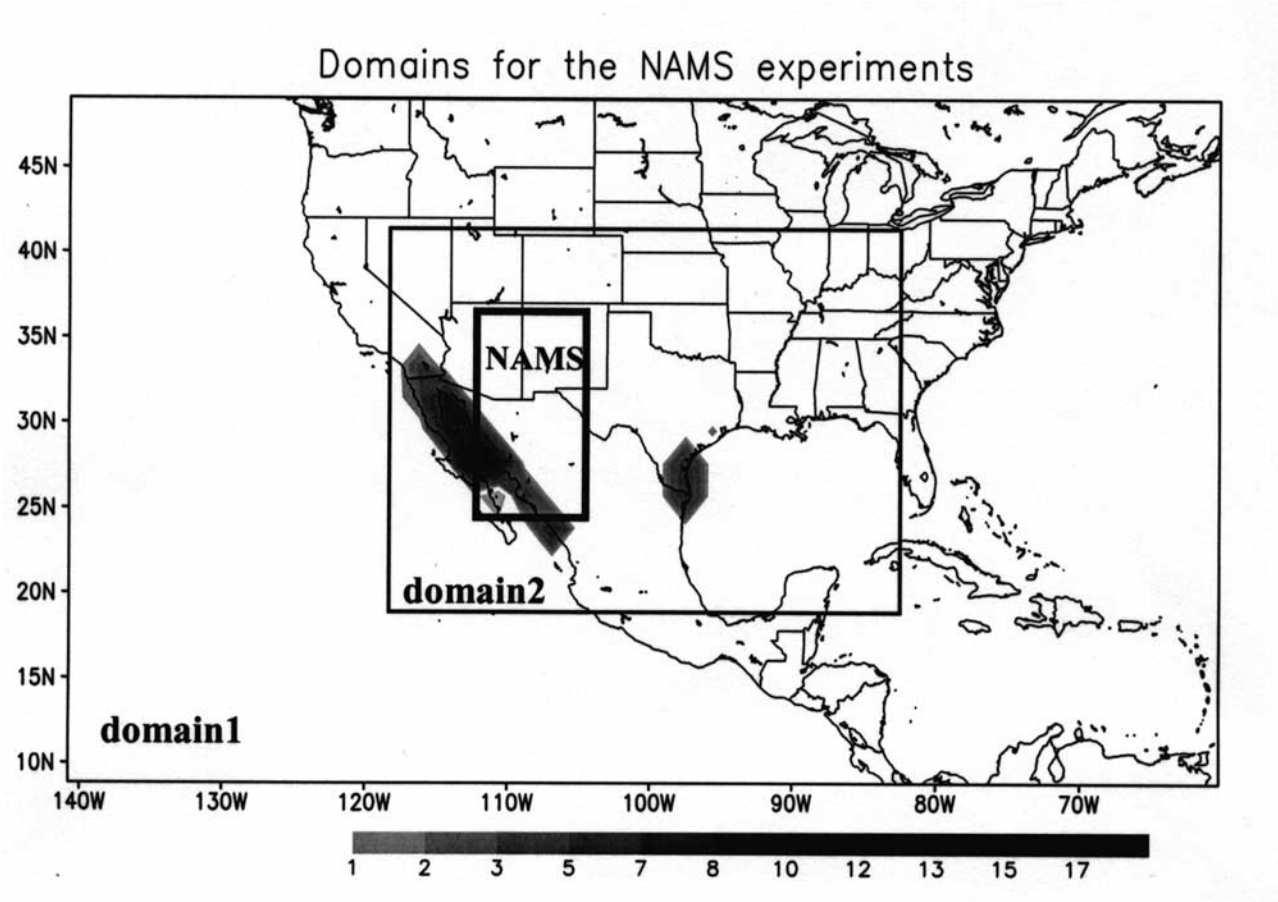

Figure 1. Domains for the MM5 simulations. The outside box is the coarse grid (domain 1) with 90 km spacing and 40 × 68 points; the inner box is the nested grid (domain 2) with 30 km spacing and 100 × 70 points. The inside thick box shows the North American monsoon region used in our analyses (112°W–105°W, 24°N–36°N). The shading shows the typical noon temperature difference between the Reynolds SST and NCEP reanalysis SST in the Gulf of California.

may also influence NAMS variability [*Lo and Clark*, 2001; *Gutzler*, 2000; *Small*, 2001]. Land surface state within the NAMS region and in adjacent areas such as the Rocky Mountains may both be important.

[4] There is currently a substantial focus on understanding NAMS dynamics, with the goal of assessing the predictability of rainfall variability in this region and developing tools for prediction (e.g., North American Monsoon Experiment (NAME) Science and Implementation Plan, available at http://www.cpc.ncep.noaa.gov/products/precip/monsoon/NAME.html). Limited-area or regional climate models resolve mesoscale features, such as the topography within the NAMS region or the coastlines that surround it. Therefore, these models provide one means of studying the NAMS system and its variability. These sorts of model have been applied to various regions [e.g., *Dickinson et al.*, 1989; *Giorgi*, 1990; *Giorgi and Mearns*, 1999; *Small et al.*, 1999]. However, their application to the NAMS region has been of limited duration only [e.g., *Stensrud et al.*, 1995; *Small*, 2001; *Gochis et al.*, 2002], which we show yields only first-order information regarding their use for prediction of rainfall variability.

[5] Although regional climate models are potentially useful tools for studying features such as the NAMS, the simulations are sensitive to a variety of boundary conditions and parameterizations that must be specified by the user. Results are sensitive to grid resolution [*Giorgi and Marinucci*, 1996] and domain size [*Seth and Giorgi*, 1998]. The cumulus parameterization scheme (CPS) used also has a substantial impact on the simulation [*Wang and Seaman*, 1997; *Giorgi and Shields*, 1999], particularly in areas such as the NAMS region where convection is a key process [*Gochis et. al.*, 2002]. However, focusing on the CPS alone without attention to the radiation scheme and its impact on the radiation budget may be problematic. The surface radiation budget drives the transfer of water and energy between the surface and the atmosphere, therefore impacting boundary layer characteristics and convection [*Betts and Ball*, 1994; *Eltahir and Pal*, 1996; *Schar et al.*, 1999; *Pal and Eltahir*, 2001].

[6] The first step in using regional models to study NAMS dynamics is to identify the model domain and suite of physical parameterizations that yields the best possible simulations given a particular modeling system. This task is challenging for several reasons. First, there are many possible combinations of resolution, domain extent, and physical parameterizations. Second, as we show here, the optimal setup for one set of synoptic conditions or time

period may not be the same as for another. And third, model runs are computationally expensive, so it is not possible to complete 100's of season long simulations. Given these three considerations, it is not possible to employ formal optimization techniques used in other fields [e.g., *Sorooshian et al.*, 1993].

[7] Even though it is not possible to compare all possible model arrangements, it is useful to compare the results from simulations that include different key parameterizations [e.g., *Pal and Eltahir*, 2001; *Giorgi and Shields*, 1999]. *Gochis et al.* [2002] took a first step along this path for simulations of the NAMS. They compared how different CPS influenced MM5/OSU model simulations of the NAMS during July 1999. They found substantial differences between the simulations that included different CPS and concluded that the Kain-Fritsch CPS yielded the most realistic surface and upper air-fields. We present very different results here, based on analysis of simulations from 1999 and 2000, and comparisons between different radiation schemes.

[8] In this study, we compare MM5/OSU simulations with different combinations of convection and radiation schemes, furthering the work of *Gochis et al.* [2002]. Our goal is to examine how accurately the MM5/OSU modeling system simulates intraseasonal and interannual variability of the NAMS, and how the accuracy depends on the model setup. We compare the model output with NCEP/NCAR reanalysis circulation, moisture transport, and vertical profiles of θ_e and against two different precipitation data sets (CPC and CMAP). Our study is based on a year with above-normal precipitation (1999) and one with below-normal precipitation (2000).

[9] The paper is organized as follows. Section 2 introduces the model used in this study and the different physical parameterization compared. The observed differences in the NAMS between 1999 and 2000 are discussed in section 3. The simulated seasonal evolution of NAMS using different parameterizations are compared with observations in section 4, while the simulated interannual variability is described in section 5. This is followed by a discussion and conclusions.

2. Model and Simulations

[10] We used NCAR's MM5 model version 3.4 coupled to the Oregon State University (OSU) land surface model in this study. MM5 is a limited area, sigma coordinate, nonhydrostatic, mesoscale atmospheric model [*Grell et al.*, 1994]. The OSU land surface scheme calculates the water and energy balance for a single canopy and four soil layers [*Chen and Dudhia*, 2001]. Earlier versions of MM5 model have been used for NAMS simulations, but temporal variations in land surface conditions [*Stensrud et al.*, 1995] and SSTs [*Small*, 2001] were not represented.

2.1. Domain Selection, Period of Simulation, and Boundary Conditions

2.1.1. Resolution and Placement of Model Domain

[11] We selected a 90-km coarse grid that permits a realistic representation of low-level flow from both the Pacific/Gulf of California and the Gulf of Mexico regions (See Figure 1). A 30-km two-way nested grid is centered over the NAMS region, and allows for an improved representation of the region's complex topography and associated spatial variability of surface characteristics.

Table 1. Model Options and Design of Numerical Experiments

Physics Option	Model Setup
Explicit microphysics	Simple Ice [*Grell et al.*, 1994]
Land-Surface Model	OSU [*Chen and Dudhia*, 2001]
P.B.L.	MRF [*Hong and Pan*, 1996]
Radiation	Cloud Rad. Scheme [*Grell et al.*, 1994]
	CCM2 Rad. Scheme [*Hack et al.*, 1993]
	RRTM Longwave scheme [*Mlawer et al.*, 1997]
Cumulus	Kain-Fritsch [*Kain and Fritsch*, 1993]
	Grell [*Grell et al.*, 1994]
Numerical Experiment	**Design**
Exp1 (KF-CCM2)	Kain-Fritsch and CCM2 Rad. Scheme
Exp2 (KF-Could)	Kain-Fritsch and Cloud Rad. Scheme
Exp3 (KF-RRTM)	Kain-Fritsch and RRTM Longwave Scheme
Exp4 (Grell-CCM2)	Grell and CCM2 Rad. Scheme
Exp5 (Grell-Cloud)	Grell and Cloud Rad. Scheme
Exp6 (Grell-RRTM)	Grell and RRTM Longwave Scheme

2.1.2. Period of Simulation

[12] We completed simulations that cover the period June 1 through July 31 in 1999 and 2000. The initial conditions (see below) were specific to June 1 in each year. We completed two extra simulations in both 1999 and 2000 with one model arrangement (Grell-RRTM) to assess internal variability within the model. These simulations were started 12 and 24 hours later than the original Grell-RRTM simulation.

2.1.3. Consistency of Boundary Conditions and Land-Ocean Mask

[13] The initial conditions and time-varying boundary conditions for the coarse domain are taken from the NCEP/NCAR reanalysis data sets [*Kalnay et al.*, 1996]. Initial conditions include atmospheric and surface fields, the latter including soil moisture and temperature. The time-varying boundary conditions include (1) atmospheric fields at the lateral boundaries of the coarse domain and (2) SSTs throughout the coarse and fine domains. We found that the relatively high resolution (30 km) MM5 land-ocean mask was inconsistent with the coarse-resolution (2.5°) time-varying sea surface temperature (SST) boundary conditions from NCEP. There were extensive coastal areas treated as "ocean" in the MM5 model that were considered land in the coarser resolution NCEP data from which SSTs are extracted. This yields SSTS > 40°C during the middle of the day in some coastal areas (Figure 1), which produces very high latent heating and precipitation over nearby elevated topography. The problem was most severe along the Gulf of California, an area critical for simulating the NAMS. Here we use Reynold's SST data [*Reynolds and Smith*, 1994] over the Gulf of California and parts of the Gulf of Mexico, in locations where the NCEP data actually represents land surface temperatures. Replacing the high NCEP surface temperatures with realistic SSTs greatly improves the simulated precipitation in coastal areas (not shown).

2.2. Convection and Radiation Parameterizations

[14] We now describe the different convection and radiation schemes compared in this study (Table 1). We provide enough information to support the discussion of our results, and provide references to the original sources that describe

these schemes in detail. We chose the two CPS (Grell and Kain-Fritsch) that are recommended for simulations with 30-km grid spacing [*Dudhia et al.*, 2001] and the three most sophisticated radiation schema.

2.2.1. Grell CPS Scheme

[15] The Grell scheme is a simplified version of the *Arakawa and Schubert* [1974] cloud ensemble parameterization [*Grell*, 1993; *Grell et al.*, 1994]. It represents a single cloud with a coupled updraft and downdraft. The convective flux is constant with height because there is no mixing between the updraft and downdraft and with the surrounding atmosphere. The Grell scheme is activated when the grid-scale vertical velocity lifts stable layers past the level of free convection. The convective precipitation is proportional to the condensation in the updraft, the mass flux of the updraft, and an efficiency parameter.

2.2.2. Kain-Fritsch CPS

[16] The Kain-Fritsch convective parameterization scheme is based on the model of *Fritsch and Chappell* [1980]. Like the Grell scheme, both an updraft and downdraft are explicitly represented in the KF CPS. Convection is triggered when the column is unstable and the grid-resolved vertical velocity is sufficient to overcome buoyancy forces. The precipitation rate is a function of an efficiency factor and the vertical fluxes of liquid and vapor. The latter is determined based on grid-scale CAPE, which is eliminated via convection on the hourly timescale.

2.2.3. CCM2 Radiation Scheme

[17] This radiation scheme was used in NCAR's CCM2 global model [*Hack et al.*, 1993]. It estimates the clear and cloudy sky influence on shortwave and longwave radiation, integrated over multiple spectral band. Clouds exist whenever the relative humidity exceeds a threshold. The amount of cloud liquid water at any model level is then prescribed to a preset value. Therefore, there are no explicit interactions between the amount of condensation and the optical thickness of clouds.

2.2.4. Cloud Radiation Scheme

[18] This scheme is similar to CCM2 in that the radiative effects of clear and cloudy sky on shortwave and longwave are estimated. However, the amount of cloud water is explicitly linked to the condensation calculated during the simulation.

2.2.5. RRTM Long-Wave Scheme

[19] This is combined with the cloud scheme to provide more detailed calculations of long-wave radiation transfer [*Mlawer et al.*, 1997]. It is the Rapid Radiative Transfer Model and uses a correlated-k model to represent the effects of the detailed absorption spectrum taking into account water vapor, carbon dioxide and ozone. It is implemented in MM5 to also interact with the model cloud and precipitation fields in a similar way to the cloud-radiation scheme.

3. Observed State of the North American Monsoon System in 1999 and 2000

[20] It is necessary to understand the observed features of the NAMS in the two simulated years (1999, 2000) before comparing model results to observations. We used atmospheric circulation, moisture transport, and vertical θ_e profile data from the NCEP/NCAR reanalysis product [*Kalnay et al.*, 1996] and precipitation data from Climate Prediction Center (CPC) data sets [*Higgins et al.*, 1996]. The CPC data consists of 6000 quality gauge stations from the United States Cooperative Observing Network, interpolated onto a 0.25° longitude by 0.25° latitude grid. Due to some missing gauge data in Mexico (discussed below), the CPC Merged Analysis of Precipitation (CMAP) data is also used. This data set is the product of merging five kinds of satellite estimates (GPI, OPI, SSM/I scattering, SSM/I emission, and MSU). The enhanced file also includes blended NCEP/NCAR reanalysis precipitation values. The resolution of the data is 2.5° × 2.5° [*Xie and Arkin*, 1996].

3.1. Atmospheric Circulation and Moisture Transportation at Lower Level

[21] In June 1999, central Mexico and the southern U.S. were dominated by anticyclonic flow at low levels (700 hPa) (Figure 2a). The entire southwestern U.S. was dominated by southwesterlies. As a result of this circulation, the eastern Pacific and Gulf of California were the primary moisture sources for the northern NAMS region. Moisture from the Gulf of Mexico does not contribute to the NAMS region. Instead, flow from the Gulf of Mexico is transported into southern Mexico and into the southeastern U.S. By July (Figure 2b), the high-pressure ridge shifted northward, yielding a strong flow of moisture from the Gulf of Mexico into the NAMS region. Moisture transport from the Gulf of California and Pacific decreased substantially compared to June. From June to July, the westerlies decrease over the southern United States and Mexico (Figure 2c).

[22] The differences between circulation and moisture transport in 1999 and 2000 shows the intensity of interannual variability in this region. In June 2000, the anticyclonic flow over the NAMS region is shifted further north compared to June 1999 (Figure 3a). Moisture transport from the Gulf of Mexico is roughly similar to that in 1999, but flow from the Pacific and Gulf of California into the NAMS region is reduced (not shown). The contrasts between 1999 and 2000 are much more dramatic in July. In July 2000, the high is shifted northward and is much stronger than in 1999 (Figure 3b). This greatly reduces moisture transport from the Gulf of Mexico into the NAMS region (Figure 4a). Moisture transport from the Gulf of Mexico into the Great Plains region is also reduced dramatically.

3.2. Vertical Profile and Convective Stability

[23] We calculate the vertical profile of equivalent potential temperature (EPT, θ_e) from the NCEP/NCAR reanalysis data, averaged over the NAMS and Great Plain (GP) regions (102°–95°W, 30°–36°N). In both years and regions, the EPT decreases with height from the surface up to the 500 hPa level, showing that the lower troposphere is unstable (Figure 5a). EPT increases with height above 500 hPa, indicating stable conditions. In the NAMS region, the vertical profiles are rather different in the wet (1999) and dry (2000) years. In the wet year, the vertical gradient of EPT is enhanced, indicating stronger convective instability during this year (Figure 5a). The difference is primarily the result of warmer and/or wetter conditions

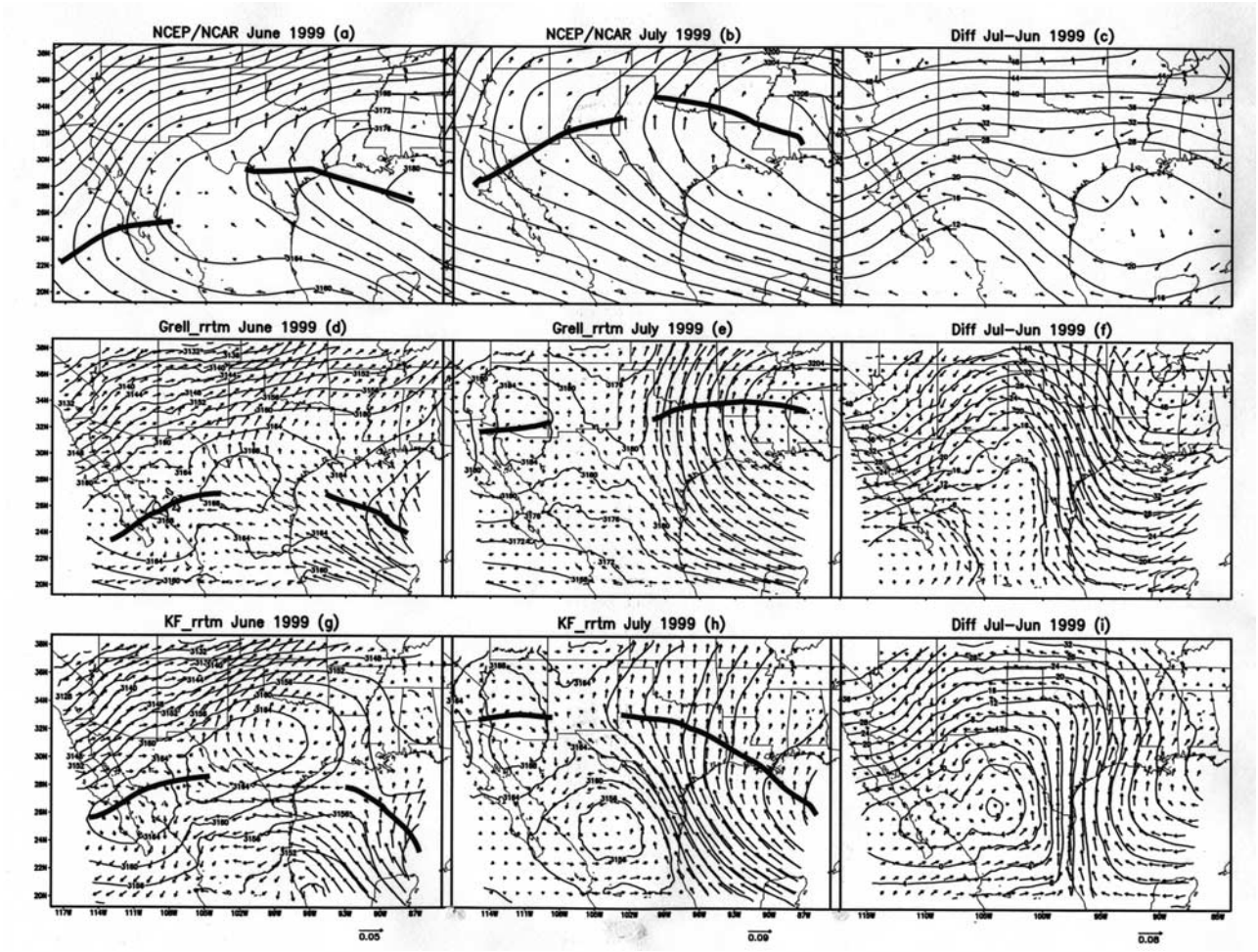

Figure 2. Monthly mean 700-hPa circulation from NCEP reanalysis data and MM5 simulations for 1999. The vectors show 700-hPa moisture transport (u*q; v*q) (unit: kg/kg*m/s); the contours indicate geopotential height (unit: gmp), and the thick lines indicate the location of high-pressure ridge. (a) June, (b) July and (c) July–June difference from NCEP reanalysis; (d) June, (e) July and (f) July–June difference in the Grell-RRTM experiment; (g) June, (h) July and (i) July–June difference in the KF-RRTM experiment.

near the surface, which is in accord with the observed differences in circulation between the two years (Figure 4a). The GP EPT gradient is similar in 1999 and 2000, and is of similar magnitude to the instability observed in the NAMS region.

3.3. NAMS Onset and Precipitation

[24] In 1999, there is a sharp onset of precipitation in the NAMS region in the beginning of July in both the CPC and CMAP data sets (Figure 6). The pattern is different in 2000. There is no sharp onset of rainfall, and the peak precipitation occurs toward the end of June.

[25] In June 1999, the greatest precipitation is observed (CPC and CMAP) over the GP (Figure 7a). The pattern of precipitation across the southern United States and Mexico changes dramatically with the onset of NAMS precipitation. The precipitation maximum shifts from the GP region in June to the NAMS region in July (Figure 7b and Figure 10a), although a local maximum exists over the Florida panhandle. These month-to-month changes in 1999 follow the typical seesaw pattern observed between these two regions [*Higgins et al.*, 1999]. The rainfall patterns are very different in 2000. The June rainfall maximum over the GP is more diffuse, extending into the NAMS region. From June to July (Figure 8b), the rainfall decreases substantially throughout the entire southern United States and northern Mexico (Figure 10b). Even the NAMS region is drier in July than in June. The typical monsoon onset does not occur in 2000. The 2000 CPC data in southern Mexico is clearly incorrect, as this is the only interval we found when CPC and CMAP strongly differ.

[26] The intraseasonal (June to July) and interannual variations (1999 to 2000) in precipitation are clearly linked with the observed differences in atmospheric circulation between these 2 years. For example, the strong anticyclone that dominates the southern United States in July 2000 (See Figure 3a) inhibits moisture transport into the region, modifying the vertical profiles of moisture and temperature, and therefore precipitation. An accurate description of atmospheric circulation is necessary for simulating the

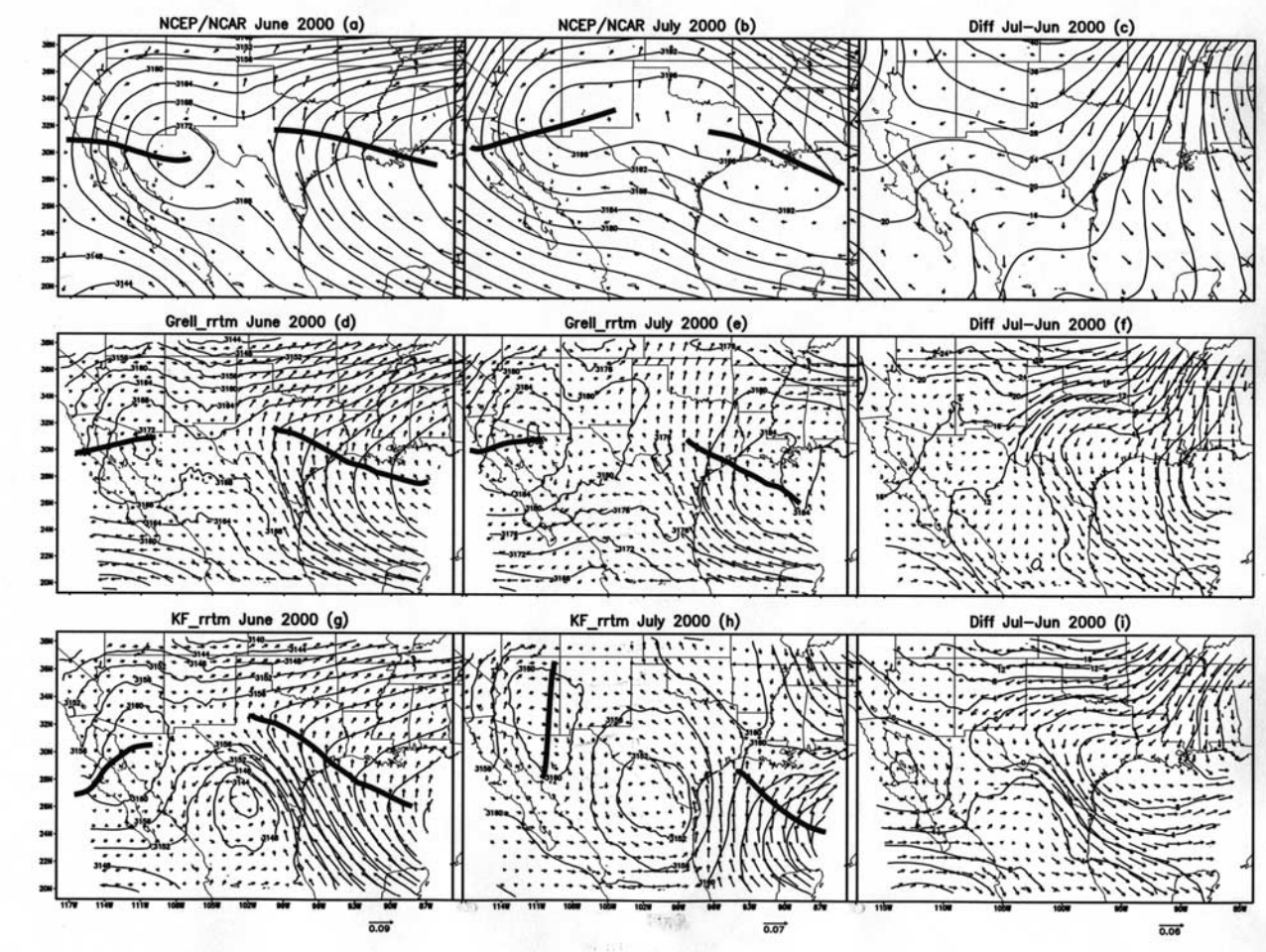

Figure 3. Same as Figure 2 but for 2000.

spatial and temporal variation in summertime precipitation in the southern United States and Mexico.

4. Influence of Convection and Radiation Schemes in the Simulated NAMS

[27] We now compare the evolution of the NAMS in 1999 and 2000 as simulated by MM5-OSU model with six combinations of CPS (KF and Grell) and RAD schemes (CCM2, Cloud, and RRTM). All experiments were initialized on 0000 UTC 1 June and integrated continuously through 0000 UTC 31 July.

4.1. Atmospheric Circulation and Moisture Transportation at Lower Level

[28] First, we compare the large-scale atmospheric circulation and resulting moisture transport in the six MM5 simulations with the comparable fields from the NCEP reanalysis. We focus on the low-level flow (700 hPa), as the month-to-month and year-to-year differences are dramatic at this level. We chose the 700 hPa level because it is the lowest level that is above the surface throughout the NAMS region. We have compared the 700 hPa fields to those at lower levels (not shown). The flow and moisture transport at 700 hPa is representative of that throughout the lower troposphere. We focus on the Grell-RRTM and KF-RRTM experiments, and point out important differences between the other simulations where they exist.

[29] In June 1999, the Grell-RRTM and KF-RRTM simulations generally represent the anticyclonic flow observed over the southern U.S. and Mexico (Figures 2d and 2g). However, there are substantial differences in both the location and the intensity of highs between the two experiments, and between the experiments and observations. In both simulations, the high-pressure centers are stronger and farther northeast than in the NCEP reanalysis. This reduces moisture transport from the Gulf of Mexico into the southern GP, compared to the observations. The anticyclonic flow is stronger in the KF-RRTM simulation than in the Grell-RRTM simulation, yielding low-level moisture transport over the southern GP that is opposite in direction from NCEP. In all simulations, the circulation has much more fine-scale structure than in NCEP/NCAR reanalysis fields. This is related to the higher resolution of the MM5-OSU model. We do not know if the added details are realistic.

[30] In July 1999, the simulated circulation is more similar to observed than in June (Figures 2e and 2f). Both experiments represent the circulation changes associated with the onset of the NAMS: the anticyclonic flow center over the Sierra Madre Occidental shifts northward into the southwestern United States. This enhances moisture transport from the Gulf of Mexico into the NAMS region,

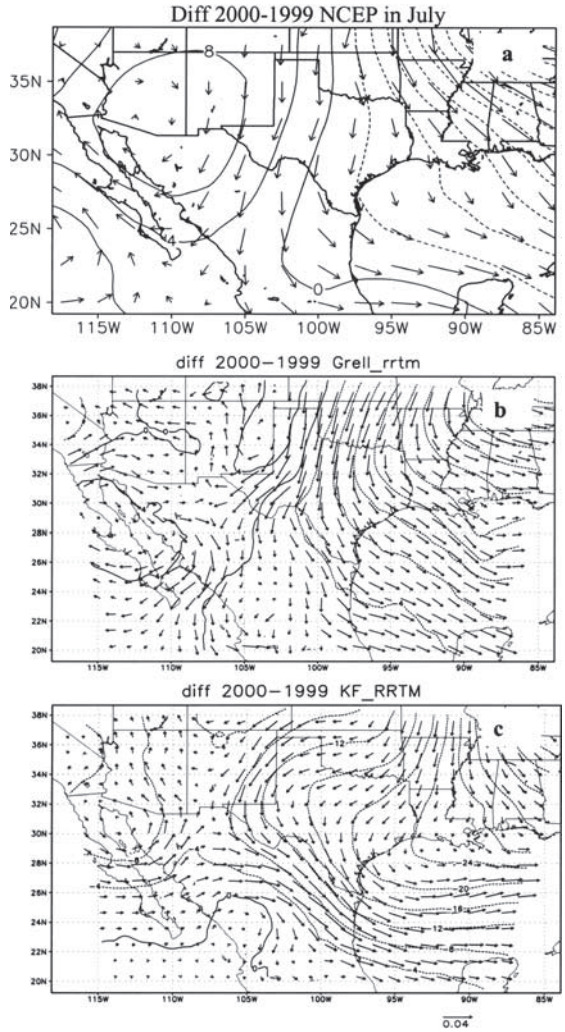

Figure 4. The 700-hPa differences between July 2000 and July 1999. The vectors show moisture transport (u*q; v*q) (unit: kg/kg*m/s); the contours indicate geopotential height (unit: gmp). (a) NCEP. (b) Grell-RRTM. (c) KF-RRTM.

although the simulated moisture transport does not extend as far west as in the reanalysis. In the KF-RRTM, a low pressure exists over Mexico that is not observed in the NCEP reanalysis or the Grell-RRTM experiment. This low yields very high precipitation in this region that is not observed in the high-resolution CPC data set. Differences between the six simulations are numerous. The simulations that include the CCM2 radiation scheme exhibit anomalously strong anticyclonic flow over Arizona (AZ) and New Mexico (NM), precluding moisture transport from the Gulf of Mexico into the NAMS region (not shown).

[31] The July−June difference in Grell-RRTM (Figure 2f) is consistent with the NCEP/NCAR reanalysis field (Figure 2c). The difference field in KF-RRTM (Figure 2i) is also similar, but includes relative cyclonic flow that is too strong over Mexico.

[32] In 2000, the circulation in both June and July in Grell-RRTM (Figures 3d and 3e) is similar to observed (Figures 3a−3c). In contrast, the circulation simulated in the KF-RRTM run is dramatically different than observed (Figures 3g and 3h). In KF-RRTM, Mexico is dominated by anomalously strong cyclonic flow, just as was simulated for July 1999. This structure enhances moisture convergence over Mexico yielding precipitation that is much stronger than observed (see below).

[33] The 2000 difference field between July and June from the Grell-RRTM simulation (Figure 3f) is similar to

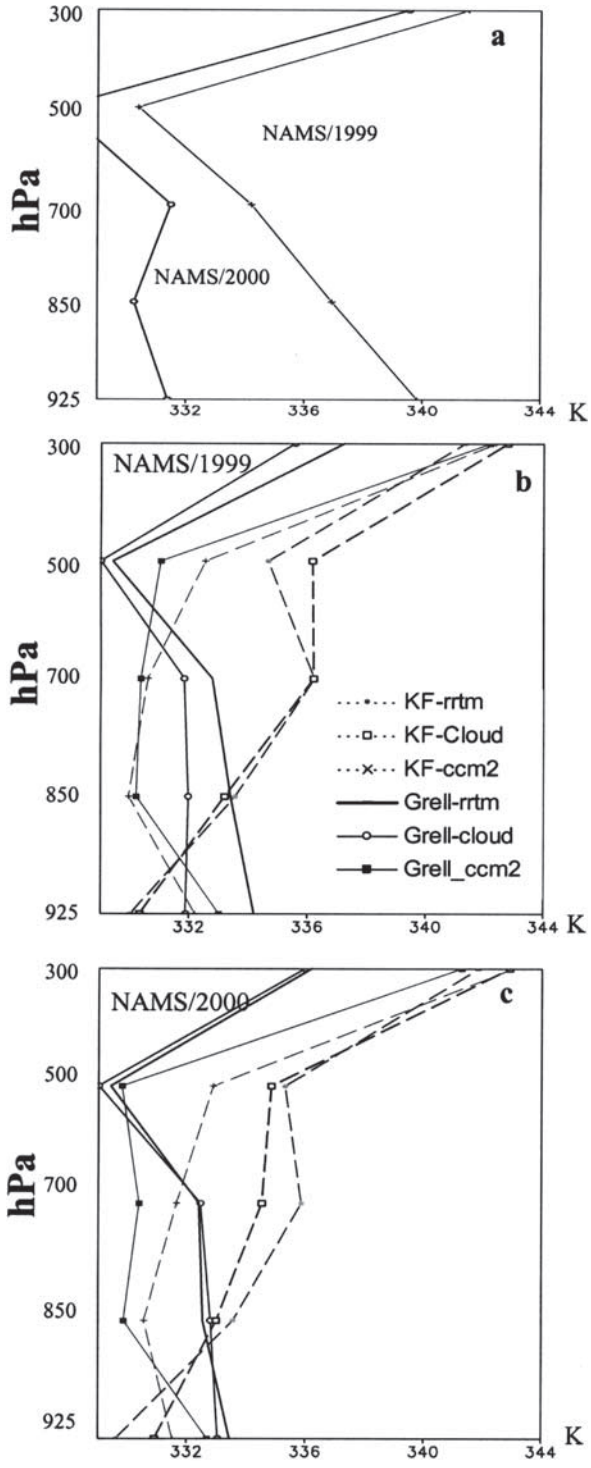

Figure 5. Profiles of monthly mean equivalent potential temperature (θ_e) averaged over the NAMS and Great Plains (GP) regions. (a) NCEP reanalysis. (b) NAMS 1999. (c) NAMS 2000.

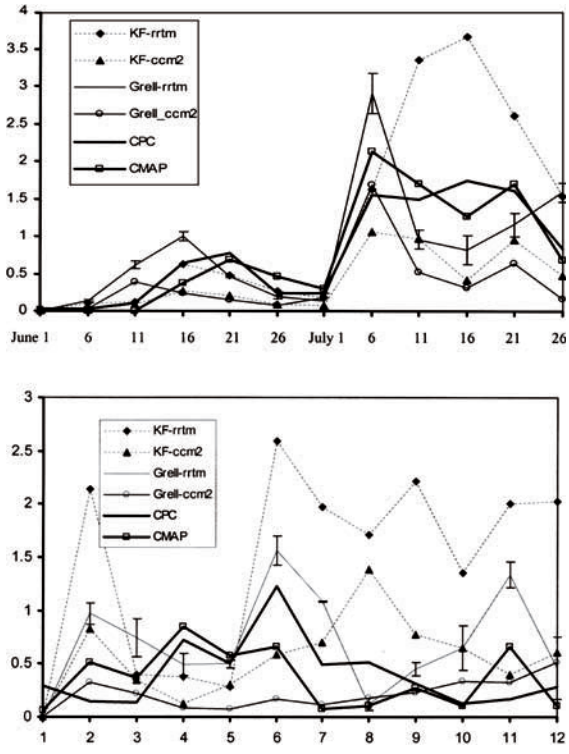

Figure 6. Time series of observed and simulated precipitation over the NAMS region for the period June 1 through July 31, for (a) 1999 and (b) 2000. All values are five-day averages. Not all simulations are shown for clarity. The error bars on the Grell-RRTM line show the range of precipitation value simulated in the three-member ensemble completed with this model setup.

the reanalysis: There is a decrease in moisture transport from the Gulf of Mexico into the southern U.S. This feature is not simulated as closely in the KF-RRTM simulation (Figure 3i), but it is partially represented. In addition, the KF-RRTM difference field includes more flow into the NAMS region from the Pacific than in the NCEP reanalysis or in the Grell-RRTM simulation.

4.2. Vertical Profile and Convective Stability

[34] We now compare the July vertical profiles of θ_e in the six simulations to those in the NCEP/NCAR reanalysis (Figure 5a). In both years, the vertical profiles of θ_e (Figures 5b and 5c) fall into three distinct groups: (1) Grell-Cloud and Grell-RRTM; (2) KF-Cloud and KF-RRTM; and (3) Grell-CCM2 and KF-CCM2. The vertical profiles from the Grell-Cloud and Grell-RRTM experiments are similar to those in the reanalysis: the θ_e gradient is negative up to 500 hPa and positive above that level. Averaged throughout July, the lower troposphere is convectively unstable in these simulations. In contrast, the θ_e vertical gradient is positive throughout the profile in the KF-Cloud and KF-RRTM simulations, so the profile is stable. The profiles from simulations with CCM2 radiation fall in the middle. The fact that the CCM2 lines are so similar shows that this radiation scheme exerts a strong influence on the simulated fields (relative to the CPS). In all six experiments, there are virtually no differences between 1999 and 2000, which is in stark contrast to the year-to-year differences included in the NCEP reanalysis.

4.3. NAMS Precipitation

4.3.1. Time Series

[35] In 1999, all six simulations show a dramatic rise in precipitation in early July (Figure 6a), as observed in the CPC and CMAP precipitation data sets. Following this initial rise, the precipitation rate in the Grell-RRTM and Grell-Cloud simulations drops off slightly, similar to the observations. In contrast, the precipitation in the KF-Cloud and KF-RRTM cases continues to grow until the middle of July, to a maximum of 3.5 mm/day. In simulations with CCM2 radiation, the decrease following NAMS onset is greater than observed.

[36] In 2000 (Figure 6b), the Grell-RRTM and Grell-Cloud simulations follow the observed time series most closely, rising for a 10-day interval at the end of June and subsequently decreasing. The precipitation in the KF-Cloud and KF-RRTM cases also rises during late June, but does not decrease in July as observed. In 2000, the simulations with CCM2 follow different progressions: The peak in KF-CCM2 precipitation is later than observed and there is virtually no precipitation in the Grell-CCM2 case. In almost all simulations, there is a short-duration rise at the beginning of June that is not observed in the CPC or CMAP data sets. The source of this bias is unknown.

[37] Figure 6 shows the variations in the three-member ensemble of simulations produced with the Grell-RRTM setup, which is measure of internal model variability. The differences between the three Grell-RRTM simulations are typically small, at least compared to the differences in simulated rainfall that arise from using different convection or radiation schemes.

4.3.2. Magnitude of Precipitation

[38] In July 1999, the magnitude of precipitation in the KF-Cloud and KF-RRTM is almost twice the CPC observed precipitation and is also much higher than the CMAP observed value (Figure 9, Table 2). The simulated precipitation in the Grell-RRTM simulation is virtually the same as CPC and is slightly lower than CMAP. The other three cases (KF-CCM2, Grell-CCM2 and Grell-Cloud) have only half of the observed precipitation. All six simulations show the observed precipitation increase from June to July. There is a substantial difference in July minus June precipitation between the CPC and CMAP data sets. The Grell-RRTM simulation yields the July–June difference that is closest to both values.

[39] In July 2000, the magnitude of precipitation in the KF-Cloud and KF-RRTM cases is many times greater than observed (Figure 9, Table 2). The Grell-RRTM and Grell-Cloud setups also produce too much precipitation, but the

Figure 7. (opposite) The 1999 June and July mean-monthly precipitation from observations (CPC CMAP) and MM5 simulations (Grell-RRTM and KF-RRTM) over land (unit: cm/month): CPC for (a) June and (b) July; CMAP for (c) June and (d) July; Grell-RRTM for (e) June and (f) July; and KF-RRTM for (g) June and (h) July.

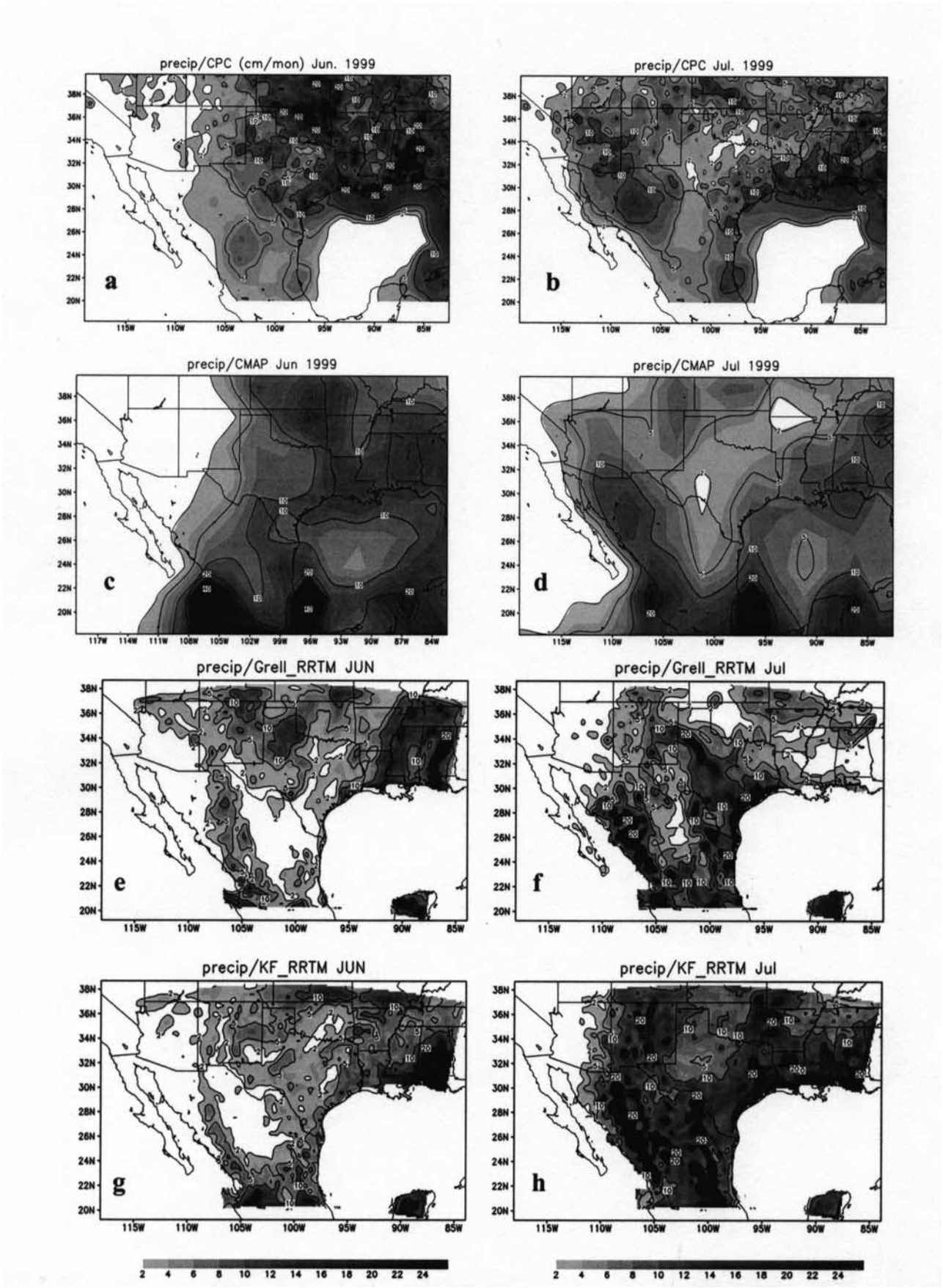
precip/CPC (cm/mon) Jun. 1999
a
precip/CPC Jul. 1999
b
precip/CMAP Jun 1999
c
precip/CMAP Jul 1999
d
precip/Grell_RRTM JUN
e
precip/Grell_RRTM Jul
f
precip/KF_RRTM JUN
g
precip/KF_RRTM Jul
h
2 4 6 8 10 12 14 16 18 20 22 24
2 4 6 8 10 12 14 16 18 20 22 24

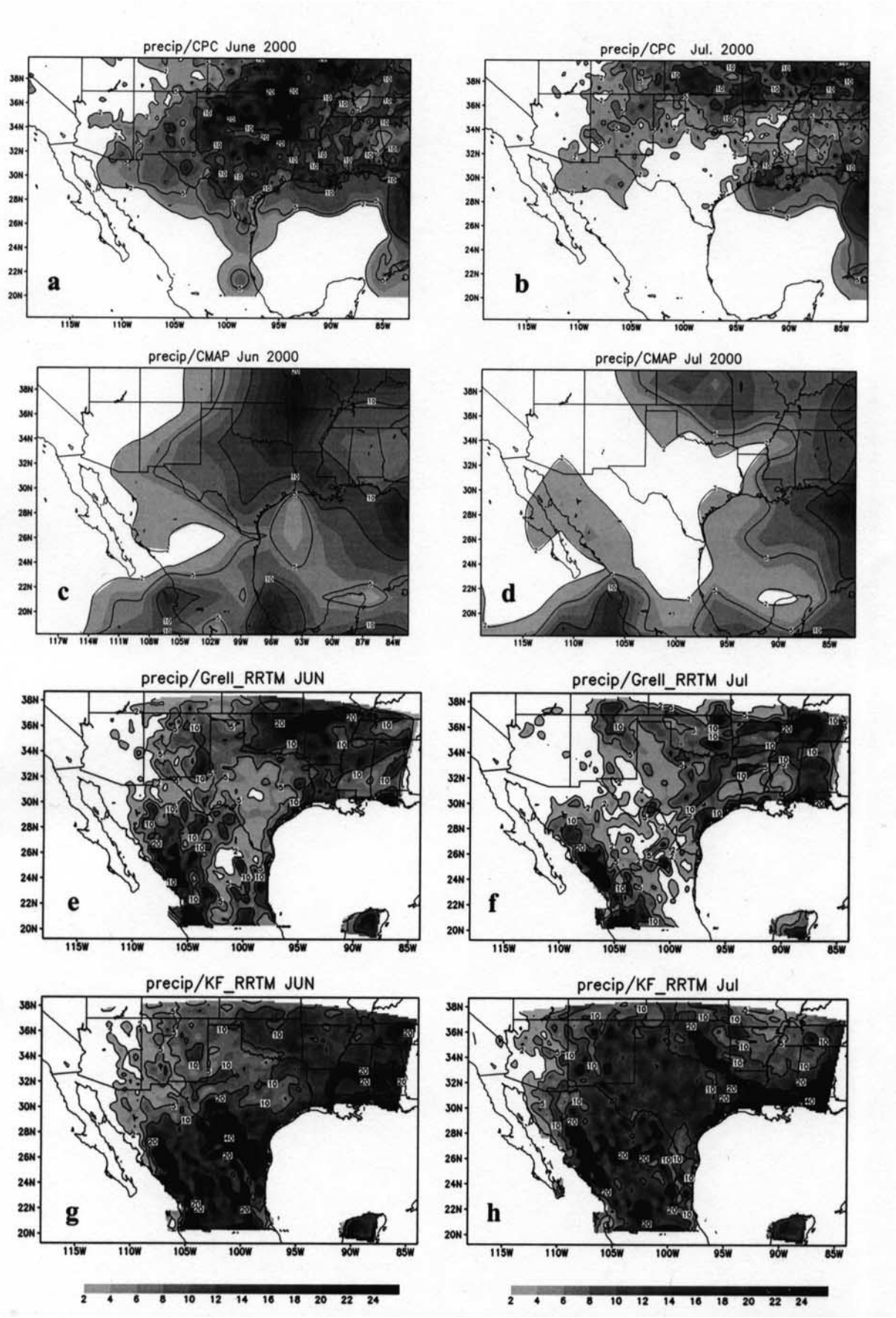

Figure 8. Same as Figure 7, but for 2000.

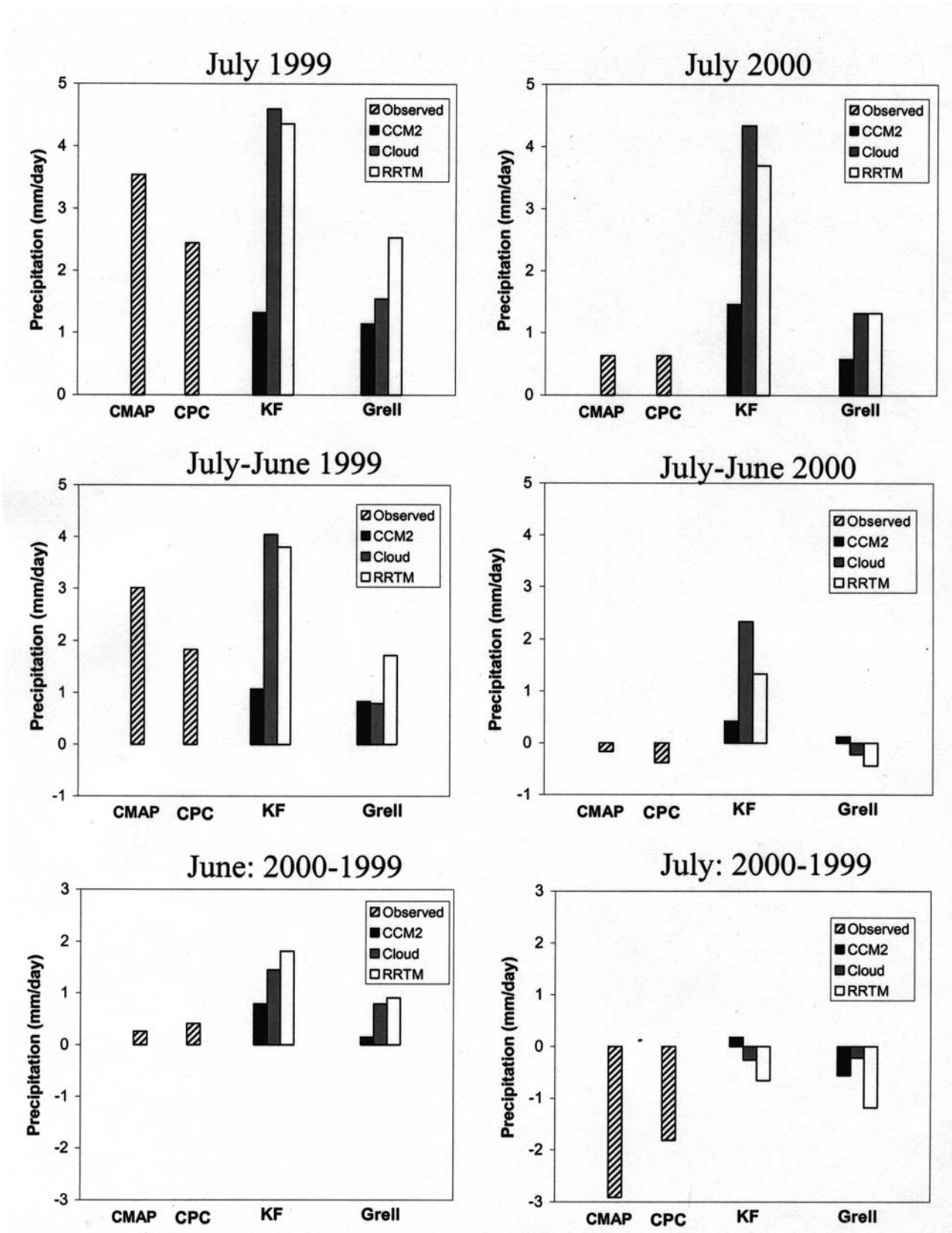

Figure 9. Mean monthly precipitation throughout the NAMS region from observations (CMAP and CPC) and all six simulations. Plots show July precipitation (1999 and 2000); July minus June differences (1999 and 2000); and 2000–1999 differences (June and July). The simulations are grouped by CPS and the pattern within each bar shows the radiation scheme used.

Table 2. Comparison of Observed Precipitation Over the Entire NAMS Region (112–105°W, 24–36°N) With the Experiments in 1999 and 2000 (mm/day)[a]

		CMAP	CPC	KF-CCM2	KF-Cloud	KF-RRTM	Grell-CCM2	Grell-Cloud	Grell-RRTM
	June	0.53	0.61	0.25	**0.56**	**0.56**	0.31	0.75	0.82
1999	July	3.54	2.44	1.32	4.60	4.36	1.14	1.54	**2.53**
	July June	3.01	1.83	1.07	4.04	3.80	0.83	0.79	**1.71**
	June	0.79	1.02	**1.04**	2.01	2.37	0.46	1.54	1.73
2000	July	0.66	0.63	1.46	4.34	3.70	**0.58**	1.32	1.32
	July June	−0.16	−0.38	0.42	2.33	1.33	0.12	−0.22	**−0.44**
2000–1999	June	0.26	0.41	0.79	1.45	1.81	**0.15**	0.79	0.91
	July	−2.91	−1.81	0.18	−0.26	−0.66	−0.56	−0.22	**−1.18**

[a]Bold numbers indicate experiment that is closest to the CPC value.

offset is not as great. The precipitation amount in the Grell-CCM2 simulation is closest to the observed amount.

[40] The observed decrease in NAMS precipitation between June 2000 and July 2000 is opposite of the usual pattern. The KF-Cloud and KF-RRTM experiments do not represent this atypical pattern: They predict an increase in precipitation from June to July that is nearly as large as in 1999 (Figure 9, Table 2). In contrast, the Grell-RRTM and Grell Cloud simulations show this atypical decrease in rainfall between July and June, and the magnitude of the decrease is similar to the observations (∼−0.3 mm/day). The Grell-CCM2 precipitation difference is also similar to observed, which is consistent with the fact that this model setup always yields very little precipitation.

4.3.3. Spatial Patterns

[41] All model arrangements that do not include the CCM2 radiation scheme produce similar patterns of precipitation in June 1999 (Figure 7). These patterns are similar to observed: strong precipitation over the GP and southeastern United States and dry conditions over northwestern Mexico and the southwestern United States. In July, the four experiments without CCM2 produce the observed heavy precipitation over New Mexico and the Sierra Madre Occidental but rainfall over AZ is underestimated. There are substantial differences between simulations. For example, the Grell-RRTM case underpredicts precipitation in the southeastern U.S. while the KF-RRTM overpredicts precipitation over most of Mexico. Table 3 shows RMSE values calculated between the simulations and observed precipitation. The Grell-Cloud and Grell-RRTM simulations yield the patterns closest to observed in July 1999, both within the NAMS region and throughout the nested domain.

[42] The differences between simulations are more apparent when we examine the month-to-month changes in rainfall. In 1999, the observed July minus June precipitation difference shows the typical GP-NAMS seesaw pattern. The Grell-RRTM case (Figure 10b) yields a similar July minus June pattern: decreased precipitation over the GP and southeastern United States and increased precipitation over the NAMS region. However, this simulation produces an unrealistic area of increasing precipitation in northeastern Mexico and southern Texas. In contrast, precipitation in the KF-RRTM simulation is rather different than observed: precipitation increases everywhere from June to July, except for a small area over Alabama. RMSE values for the July–June patterns are lower for the Grell than the KF simulations, except for the simulations that include CCM2 radiation (Table 3).

[43] In 2000, the June rainfall patterns are simulated reasonably well by all model arrangements except those including CCM2 (Figure 8). The model-to-model differences are more dramatic in July. For example, the rainfall pattern produced by the Grell-RRTM simulation is similar to observed, but the KF-RRTM pattern is too high throughout Mexico and the southwestern United States. These differences are most obvious when we look at the July minus June patterns (Figures 10b, 10d, and 10f and Table 3). Precipitation in the NAMS region and most of southern United States decreased from June to July in 2000 (Figure 10b). The Grell-RRTM simulation shows this general pattern (Figure 10d), except for a small region in Texas. In contrast, rainfall in KF-RRTM simulation is higher in July than June over most of the NAMS region and southern United States (Figure 10f). The RMSE values from the

Table 3. RMSE Calculated Between Simulated and Observed Precipitation Patterns, Over the NAMS Region and Whole Studied Areas in 1999 and 2000

		KF-ccm2	KF-cloud	KF-rrtm	Grell-ccm2	Grell-cloud	Grell-rrtm
1999 (NAMS)	July	6.99	11.16	9.83	7.3	6.71	**5.99**
	July June	**6.54**	11.22	9.78	7.48	8.70	6.65
2000 (NAMS)	July	3.44	14.73	11.13	6.11	4.50	**3.00**
	July June	3.38	9.22	7.90	5.69	4.00	**2.37**
1999 (Whole)	July	9.13	9.50	11.53	9.40	**7.68**	8.67
	July June	9.63	9.33	11.81	10.52	9.66	**8.30**
2000 (Whole)	July	7.02	9.92	17.80	4.63	6.50	**4.30**
	July June	7.50	6.34	17.02	4.79	6.60	**4.50**
2000–1999 (July)	NAMS	8.69	8.72	6.43	6.63	6.81	**5.95**
	Whole	**6.68**	7.70	11.11	7.66	6.73	8.40

Bold numbers indicate experiment that has the lowest RMSE.

Grell-RRTM are lowest for July and July–June differences in 2000, both for NAMS and the entire nested domain (Table 3).

5. Simulated Interannual Variability Between 1999 and 2000

[44] We now compare the simulated and observed variability of atmospheric circulation and precipitation. The difference in June circulation between 2000 and 1999 is that relative cyclonic flow dominated Texas and northern Mexico, yielding higher precipitation in this area in 2000 than in 1999. All six models arrangements reproduce this circulation change (not shown), and the slight increase in June precipitation in the NAMS region (Figure 9).

[45] The observed changes between 1999 and 2000 in July are more dramatic (Figure 4). 700 hPa height anomalies are negative over the GP and positive over the NAMS region. Accordingly, there is relative (2000–1999) anticyclonic flow over the NAMS region, centered over AZ. Moisture transport from the Gulf of Mexico into the GP and Mexico is greatly reduced. The observed difference in precipitation is negative throughout the NAMS region and along the entire Gulf Coast (Figures 9 and 10g). There is a slight increase in precipitation further north in the GP region.

[46] The simulated circulation and precipitation changes vary from experiment to experiment (Figures 4 and 10). The Grell-RRTM and Grell-Cloud simulations reproduce the observed circulation changes most closely, including (1) the positive-to-negative height anomalies from west to east; (2) the large-scale relative increase in northerlies and decrease in moisture transport from the Gulf of Mexico; and (3) anticyclonic flow over the NAMS region. These simulations yield decreased precipitation over the NAMS region and the Texas coast (Figure 9). The observed precipitation increase over the central GP is also reproduced, but this area of increased precipitation does extend down to the Gulf of Mexico. The Grell-RRTM simulation yields the pattern of precipitation change within the NAMS region that is most similar to observed (Table 3).

[47] The 700-hPa height differences are negative everywhere in the KF-RRTM and KF-Cloud simulations. In addition, the relative increase in northerlies is weaker than observed, as is the reduction in moisture transport from the Gulf of Mexico. There is also weak relative cyclonic flow over parts of the NAMS region. This results in positive moisture transport into the NAMS region from the Pacific. The resulting precipitation difference (2000–1999) is rather different from observed: there is an extensive area with higher precipitation over central Mexico and NM, rather than the observed decrease (Figure 10i). Accordingly, the RMSE values for these simulations are high (Table 3). The simulations that include the CCM2 radiation scheme are dominated by relative cyclonic flow over the Texas coast region and an increase in precipitation from 1999 to 2000.

6. Discussion

[48] Our comparison of simulated and observed circulation, vertical θ_e profiles, and precipitation shows that the accuracy of modeled NAMS dynamics clearly depends on the CPS and RAD parameterizations used. This result is not surprising: a variety of previous studies have highlighted the impact of physical parameterization on simulated climate in other regions. Importantly, there were notable differences between the various simulations in the representation of both the evolution of the NAMS within a year and the variability of NAMS dynamics between a wet and dry year. The model arrangement including Grell-RRTM yielded the most realistic simulation of intraseasonal and interannual precipitation variability, including both the magnitude and patterns. This is consistent with the result that the low-level circulation and moisture transport simulated by the Grell-RRTM model were most similar to observed.

[49] It is challenging to determine exactly why the Grell-RRTM simulation was the most similar to observed. The convective parameterization and radiation schema influence the simulation via numerous nonlinear pathways. However, trying to understand why one model arrangement is better than another is critical to assess what sort of physical parameterizations are optimal for predictability studies of the NAMS. In addition, this assessment can help identify what processes must be accurately represented to simulate NAMS dynamics, and therefore which processes are important in the real-world NAMS.

[50] First, we examine the energy budget of the land surface for clues of why the simulations differ. The land surface state probably plays an important role in NAMS dynamics [e.g., *Small*, 2001], so a poor representation of the surface energy balance (SEB) will likely have a negative impact on the overall simulation. The single most obvious shortcoming from a SEB perspective is that the surface incident shortwave radiation in the simulations that include the CCM2 radiation scheme is far too low. In both KF-CCM2 and Grell-CCM2, the July incident shortwave is only $\sim$170 W m^{-2} (Table 4). The incident shortwave radiation is 50% higher in the other four simulations, in accord with observed values from the NAMS region [*Small and Kurc*, 2001]. The surface temperature in the CCM2 simulations is also noticeably too low, at least compared to estimates of NAMS-averaged surface temperature from remote sensing. The low surface temperature is the obvious outcome of too little incident shortwave radiation.

[51] The CCM2 radiation problem shows that this scheme yields a climate that is too cloudy. This is an outcome of the simplicity of the CCM2 scheme as implemented in MM5. The cloud liquid water content is prescribed to a specified value (variable with height) whenever a relative humidity threshold is exceeded. There is no explicit link between condensation and the amount of radiatively-active cloud water. Not enough radiation reaches the surface because the specified cloud liquid water content is too high. The end result is that the land surface is too cool, limiting rising air, convergence and precipitation. The Cloud and RRTM schemes allow for feedbacks between condensation and the radiative thickness of clouds. This more complex coupling yields substantial improvements in the simulated climate and should be included in physically-based prediction schemes.

[52] Excluding the CCM2 simulations, the big differences between the remaining simulations can be attributed to the convective parameterizations. Differences arising from use of the Cloud versus the RRTM radiation scheme are

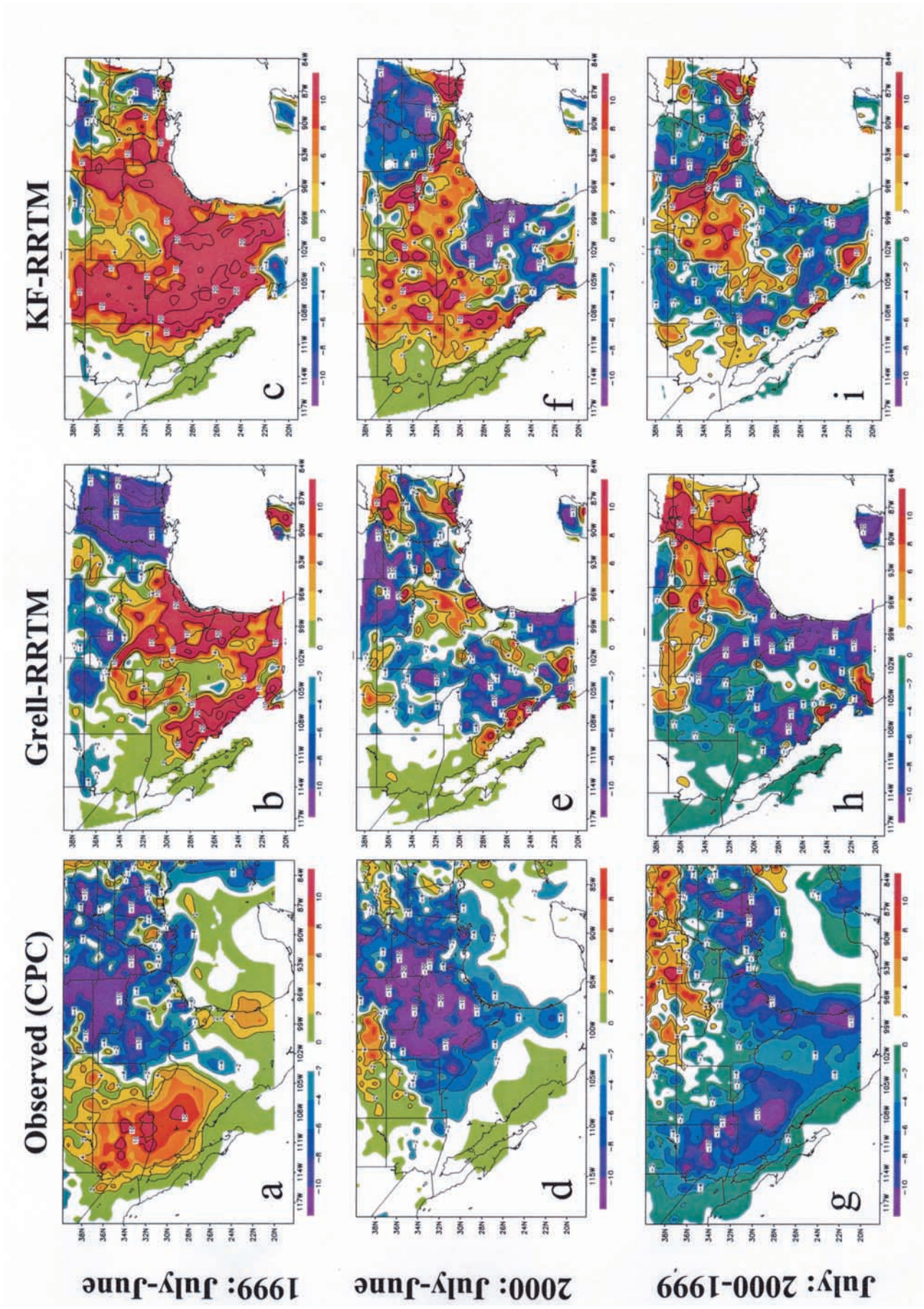
Observed (CPC)
Grell-RRTM
KF-RRTM
1999: July-June
2000: July-June
July: 2000-1999
a
b
c
d
e
f
g
h
i

Table 4. Land Surface Fluxes (Wm^{-2}), Ground Temperature (Tg in K), convective (Rc) and non-convective (Rn) Precipitation (mm/day) in NAMS Region in July

JULY		LHF	SHF	DSWR	DLWR	Tg	Rc	Rn
KF-CCM2	1999	32	43	152	362	295	0.9	0.4
	2000	39	40	155	361	294	0.9	0.5
	2000–1999	-	-	-	-	-	*0.0*	*0.1*
KF-Cloud	1999	82	90	282	405	300	3.3	1.3
	2000	83	86	268	406	299	3.3	1.1
	2000–1999	-	-	-	-	-	*−0.0*	*−0.2*
KF-RRTM	1999	66	75	246	386	298	2.3	2.1
	2000	79	67	250	382	297	2.2	1.5
	2000–1999	-	-	-	-	-	*−0.1*	*−0.6*
Grell-CCM2	1999	30	56	183	359	295	0.3	0.8
	2000	26	64	205	352	296	0.3	0.3
	2000–1999	-	-	-	-	-	*0.0*	*−0.5*
Grell-Cloud	1999	47	123	320	395	302	1.0	0.6
	2000	50	126	328	394	302	0.8	0.5
	2000–1999	-	-	-	-	-	*−0.2*	*−0.1*
Grell-RRTM	1999	53	94	286	377	299	1.1	1.4
	2000	48	111	320	368	300	0.7	0.6
	2000–1999	-	-	-	-	-	*−0.4*	*−0.8*

relatively minor in comparison. The Grell-Cloud and Grell-RRTM simulations are rather similar and differ strongly from the KF-Cloud and KF-RRTM simulations This is clearly seen in the precipitation amounts (Figure 9), vertical θ_e profiles (Figure 5), or in the time series of surface latent heat flux (Figure 11).

[53] It makes sense that using RRTM instead of Cloud yields a small difference in the simulated NAMS dynamics. The difference between these schemes is in the calculation of longwave radiation, with the RRTM scheme explicitly representing the effects of trace gases such as H_2O, CO_2, and O_3. Table 4 shows that the differences in downward longwave and shortwave radiation are minor. Both quantities are $\sim$10–20 W m^{-2} lower when the RRTM scheme is used, in both the Grell and KF experiments. The simulations including the RRTM radiation scheme yield circulation and precipitation fields that are more similar to observations than the simulations that include the Cloud scheme, at least when Grell is used (Table 3). Given that the RRTM scheme both explicitly accounts for additional physical processes and yields possibly improved simulations, this radiation scheme is the logical choice between the three tested.

[54] The final question we address is: Why does use of the Grell convective scheme yield a more realistic simulation than using the KF scheme? The KF scheme clearly yields too much precipitation in the NAMS and Gulf Coast regions (Figures 7–9 and Table 2), except in June 1999. KF rainfall is reasonable when CCM2 is used, although this is likely due to compensating errors. θ_e increases with height in the KF simulations over the NAMS region. This contrasts strongly with the NCEP profiles and those in the Grell simulations, which include a decrease to a minimum at the 500 hPa height. This difference indicates that the KF scheme is too efficient at transferring moist static energy from near the surface to the midtroposphere, removing instabilities from the column. The result suggests that the KF scheme is triggered more frequently or yields more intense convection than the Grell scheme, yielding an overprediction of precipitation (Figures 7 and 8 and Table 2). As discussed by *Gochis et al.* [2002], the KF scheme is probably triggered more frequently, because it includes a parameterization of the buoyancy effects of subgrid-scale temperature perturbations. The very high convective rainfall amounts in the KF simulations (Table 4) are additional evidence that there is too much convection in this simulation.

7. Summary

[55] In this study, we investigate how different CPS and RAD schemes influence MM5 simulations of the North American monsoon system. We focus on the simulated intraseasonal variability (June to July) and changes between a wet (1999) and a dry (2000) year. Our results show that the MM5/OSU model reproduces basic features of NAMS variability, but the accuracy strongly depend on the combination of CPS and RAD schemes. In addition, the differences in simulated rainfall between the various schema are larger than the differences that arise from internal model variability with the Grell-RRTM setup.

[56] On the intraseasonal timescale, the skill of the different model arrangements varies between 1999 and 2000. For 1999, all six model setups simulate the June-to-July increase in precipitation (monsoon onset), with the magnitude of the change closest to observed in the Grell-RRTM simulation. Only the Grell-RRTM and Grell-Cloud simulations reproduce the atypical June-to-July precipitation decrease observed in 2000. On the interannual timescale, all experiments reproduce the decrease in precipitation in July 2000, except for the KF-CCM2 experiment. Again, the magnitude and pattern of the year-to-year precipitation difference in the

Figure 10. 1(opposite) Seasonal and interannual variability of precipitation averaged over the NAMS region (unit: cm/month). July minus June difference in 1999: (a) CPC observed; (b) Grell-RRTM; and (c) KF-RRTM. July minus June difference in 2000: (d) CPC observed; (e) Grell-RRTM; and (f) KF-RRTM. July 2000 minus July 1999 difference: (g) CPC observed; (h) Grell-RRTM; and (i) KF-RRTM.

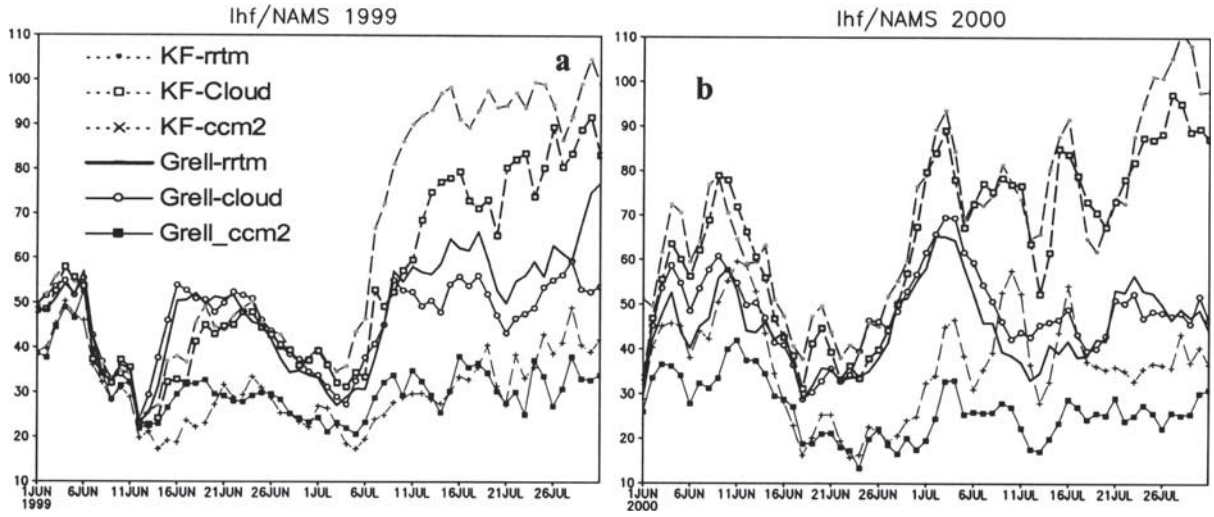

Figure 11. Time series of the surface latent heat flux (Wm^{-2}) averaged over the NAMS region in the six simulations. (a) 1999. (b) 2000.

Grell-RRTM experiment is closest to observed. Our results highlight the need for longer experiments when comparing physical parameterizations. The results presented here should be tested with experiments that sample the full range of conditions observed in the NAMS region.

[57] The CPS used has a large influence on simulated NAMS dynamics, and we recommend Grell over KF for MM5 simulations in this region. However, considering the CPS alone is not enough. The radiation parameterization used can influence the simulation as much or more than the CPS. The Cloud and RRTM radiation schemes allow for feedbacks between condensation and the radiative intensity of clouds. This explicit coupling yields substantial improvements over MM5 simulations using CCM2 radiation, in which cloud water profiles are specified.

[58] **Acknowledgments.** The authors would like to thank NCAR's Scientific Computing Division (SCD) for supporting part of calculation and providing the reanalysis data and the global SST data and Climate Prediction Center (CPC) for providing the realtime precipitation analysis data. Special thanks are extended to Sara A. Rauscher for many good suggestions for running the model and to Wei Wang and the MM5 User for answering many questions regarding the model. We also thank two anonymous reviewers for valuable comments and suggestions. This research is sponsored by NASA grant NAG5-9328 and NOAA grant NA06GP0477.

References

Adams, D. K., and A. C. Comrie, The North American Monsoon, *Bull. Am. Meteorol. Soc.*, *78*, 2197–2213, 1997.

Arakawa, A., and W. H. Shubert, Interaction of cumulus cloud ensemble with the large-scale environment, 1, *J. Atmos. Sci.*, *31*, 674–701, 1974.

Betts, A. K., and J. H. Ball, Budget analysis of FIFE-1987 sonde data, *J. Geophys. Res.*, *99*, 3655–3666, 1994.

Bryson, R. A. and E. K. Hare, *World Survey of Climatology*, vol. 2, *Climates of North America*, edited by R. A. Bryson and E. K. Hare, pp. 1–36, Elsevier Sci., New York, 1974.

Chen, F., and J. Dudhia, Coupling an advanced land-surface/hydrology model with the Penn State/NCAR MM5 modeling system, I, Model description and implementation, *Mon. Weather Rev.*, *129*, 569–585, 2001.

Dickinson, R. E., R. M. Errico, F. Giorgi, and G. T. Bates, A regional climate model for the western United States, *Clim. Change*, *15*, 383–422, 1989.

Douglas, M. W., R. A. Maddox, K. W. Howard, and S. Reyes, The Mexican monsoon, *J. Clim.*, *6*, 1665–1677, 1993.

Dudhia, J., D. Gill, Y.-R. Guo, K. Manning, and W. W. Wang, *PSU/NCAR Mesoscale Modeling System Users' Guide (MM5 Modeling System Version 3)*, June, 2001.

Eltahir, E. A. B., and J. S. Pal, Relationship between surface conditions and subsequent rainfall in convective storms, *J. Geophys. Res.*, *101*, 26,237–26,245, 1996.

Fritsch, J. M., and C. F. Chappell, Numerical prediction of convectively driven mesoscale pressure systems, I, Convective parameterization, *J. Atmos. Sci.*, *37*, 1722–1733, 1980.

Giorgi, F., Simulation of regional climate using a limited area model nested in a general circulation model, *J. Clim.*, *3*, 941–963, 1990.

Giorgi, F., and M. R. Marinucci, An investigation of the sensitivity of simulated precipitation to model resolution and its implications for climate studies, *Mon. Weather. Rev.*, *124*, 148–166, 1996.

Giorgi, F., and L. O. Mearns, Introduction to special section: Regional climate modeling revisited, *J. Geophys. Res.*, *104*, 6335–6352, 1999.

Giorgi, F., and C. Shields, Tests of precipitation parameterizations available in latest version of NCAR regional climate model (RegCM) over continental United States, *J. Geophys. Res.*, *104*, 6353–6357, 1999.

Giorgi, F., L. O. Mearns, C. Shields, and L. Mayer, A regional model study of the importance of local versus remote controls of the 1988 drought and the 1993 flood over the Central United States, *J. Clim.*, *9*, 1150–1162, 1996.

Gochis, D., W. J. Shuttleworth, and Z. L. Yang, Sensitivity of the modeled North American monsoon regional climate to convective parameterization, *Mon. Weather. Rev.*, *130*, 1282–1298, 2002.

Grell, G., Prognostic evaluation of assumptions used by cumulus parameterizations, *Mon. Weather Rev.*, *121*, 764–787, 1993.

Grell, G. A., J. Dudhia, and D. R. Stauffer, A description of the fifth-generation Penn State/NCAR mesoscale model (MM5), *NCAR Tech. Note NCAR/TN-398+STR*, 117 pp., Natl. Cent. for Atmos. Res., Boulder, Colo., 1994. (Available at http://www.mmm.ucar.edu/mm5/.)

Gutzler, D., Covariability of spring snowpack and summer rainfall across southwest United States, *J. Clim.*, *13*, 4018–4027, 2000.

Gutzler, D., and J. Preston, Evidence for a relationship between spring snow cover in North America and summer rainfall in New Mexico, *Geophys. Res. Lett.*, *24*, 2207–2210, 1997.

Hack, J. J., B. A. Boville, B. P. Briegleb, J. T. Kiehl, P. J. Rasch, and D. L. Williamson, Description of the NCAR Community Climate Model (CCM2), *NCAR Tech. Note NCAR/TN-382+STR*, 120 pp., Natl. Cent. for Atmos. Res., Boulder, Colo., 1993.

Higgins, R. W., J. E. Janowiak, and Y. Yao, A gridded hourly precipitation data base for the United States (1963–1993), *Atlas 1*, 47 pp., NCEP/NCAR/Climate Prediction Center, Washington, D.C., 1996.

Higgins, R. W., Y. Yao, E. S. Yarosh, J. E. Janowiak, and K. C. Mo, Influence of the Great Plains low-level jet on summertime precipitation and moisture transport over the central United States, *J. Clim.*, *10*, 481–507, 1997.

Higgins, R. W., Y. Chen, and A. V. Douglas, Interannual variability of the North American warm season precipitation regime, *J. Clim.*, *12*, 653–680, 1999.

Hong, S.-Y., and H.-L. Pan, Nonlocal boundary layer vertical diffusion in medium-range forecast model, *Mon Weather Rev.*, *124*, 2322–2339, 1996.

Kain, J. S. and J. M. Fritsch, Convective parameterization for mesoscale models: The Kain-Fritsch scheme, in *The Representation of Cumulus Convection in Numerical Models*, edited by K. A. Emanuel and D. J. Raymond, 246 pp., Am. Meteorol. Soc., Boston, Mass., 1993.

Kalnay, E., et al., The NCEP/NCAR 40-year reanalysis project, *Bull. Am. Meteorol. Soc.*, *77*, 437–471, 1996.

Lo, F., and M. Clark, Relationship between spring snow mass and summer precipitation in the southwestern USA associated with the North American monsoon system, *J. Clim.*, in press, 2001.

Mlawer, E. J., S. J. Taubman, P. D. Brown, M. J. Iacono, and S. A. Clough, Radiative transfer for inhomogeneous atmosphere: RRTM, a validated correlated-k model for the longwave., *J. Geophys. Res.*, *102*, 16,663–16,682, 1997.

Mock, C. J., Climatic controls and spatial variations of precipitation in western United States, *J. Clim.*, *9*, 1111–1125, 1996.

Pal, J. S., and E. A. B. Eltahir, Pathways relating soil moisture conditions to future summer rainfall within a model of the land-atmosphere system, *J. Clim.*, *14*, 1227–1242, 2001.

Reynolds, R. W., and T. M. Smith, Improved global sea surface temperature analyses using optimum interpolation, *J. Clim.*, *7*, 939–948, 1994.

Rowson, D. R., and S. J. Colucci, Synoptic climatology of thermal low-pressure systems over south-western North America, *Int.J. Climatol.*, *12*, 529–545, 1992.

Schar, C., D. L6thi, U. Beyerle, and E. Heise, The soil-precipitation feedback: A process study with a regional climate model, *J. Clim.*, *12*, 722–741, 1999.

Seth, A., and F. Giorgi, The effects of domain choice on summer precipitation simulation and sensitivity in a regional climate model., *J. Clim.*, *11*, 2698–2712, 1998.

Small, E. E., The influence of soil moisture anomalies on variability of the North American monsoon system, *Geophys. Res. Lett.*, *28*(1), 139–142, 2001.

Small, E. E. and S. Kurc, The influence of soil moisture on the surface energy balance in semiarid environments, *Tech. Completion Rep. 318*, Water Resour. Res. Inst., N.M. State Univ., Las Cruces, N.M., 2001.

Small, E. E., F. Giorgi, and L. C. Sloan, Regional climate model simulation of precipitation in Central Asia: Mean and interannual variability, *J. Geophys. Res.*, *104*, 6563–6582, 1999.

Sorooshian, S., Q. Duan, and V. K. Gupta, Calibration of rainfall-runoff models: Application of global optimization to the Sacramento Soil Moisture Accounting Model, *Water Resour. Res.*, *29*, 1185–1194, 1993.

Stensrud, D. J., R. L. Gall, S. L. Mullen, and K. W. Howard, Model climatology of the Mexican monsoon, *J. Clim.*, *8*, 1775–1794, 1995.

Tang, M., and E. R. Reiter, Plateau monsoons of the Northern Hemisphere: A comparison between North America and Tibet, *Mon. Weather Rev.*, *112*, 617–637, 1984.

Wang, W., and N. L. Seaman, A comparison study of convective parameterization schemes in a mesoscale model, *Mon. Weather Rev.*, *125*, 252–277, 1997.

Xie, P., and P. A. Arkin, Analyses of global monthly precipitation using gauge observations, satellite estimates, and numerical model predictions, *J. Clim.*, *9*, 840–858, 1996.

E. E. Small and J. Xu, Department of Earth and Environmental Science, New Mexico Institute of Mining and Technology, 801 Leroy Place, Socorro, NM 87801, USA. (esmall@nmt.edu; jxu@hwr.arizona.edu)